invasion assay により検討した。チャンバー下面に移動した細胞は、ギムザ染色液を用いて染色し、位相差顕微鏡を用いて観察した。

OEP1 結合分子を標的とした検討：

GST 蛋白融合 OEP1 発現バキュロウィルスベクターを作成し、Sf9 細胞を用いた OEP1 遺伝子産物の大量精製系を確立した。精製された OEP1 遺伝子産物をグルタチオンビーズと結合させる事により OEP1 アフィニティーカラムを作成した。OEP1 高発現膵臓がん細胞株 CFPAC1 より抽出した蛋白試料から OEP1 アフィニティーカラムを用いて、OEP1 結合分子群の精製を行った。精製された OEP1 結合蛋白を還元・アルキル化処理の後に、トリプシンを用いた蛋白消化を行って、ペプチド試料を得た。ナノフロー液体クロマトグラフィーと質量分析装置を応用することにより、試料中における網羅的発現プロファイル解析を行った（図１右）。

図１．プロテオミクス解析を用いた転移関連分子の探索・同定と機能の検討

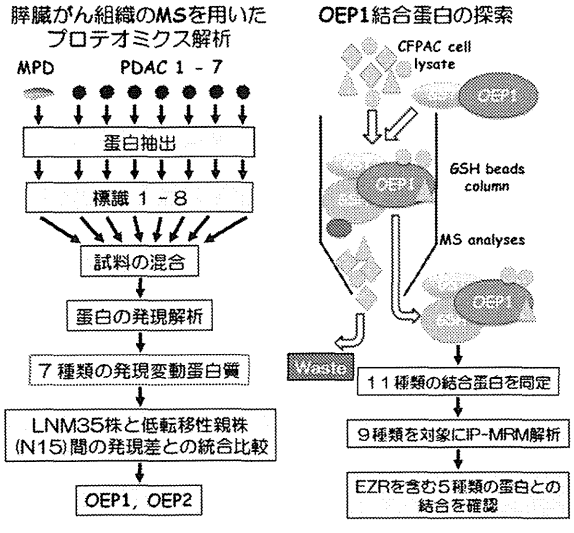

MRM 技術を用いた in vitro 結合の検証：

同定された OEP1 結合候補分子群を対象として、質量分析装置を応用した精密定量法である MRM 解析系を用いた、OEP1 アフィニティーカラムにより CFPAC1 株から精製した試料に対する検証を進めた。

膵臓がん細胞株内における OEP1 との結合の検証とシグナル解析：

OEP1 低発現膵臓がん細胞である Panc-1 を用いて、myc 標識 OEP1 を外来性に発現させ、G418 を用いて外来性 OEP1 発現細胞をセレクションし、OEP1 安定発現膵臓がん細胞株 Panc-1-OEP1-myc 細胞を樹立した。Panc-1-OEP1-myc 細胞と対照細胞（Panc-1-VC）から蛋白を抽出し、抗 myc 抗体を用いた pull down を行った。OEP1 共沈分子に対してウェスタンブロット法を用いた解析を行い、OEP1 結合候補蛋白の存在に関する検討を行った。OEP1 を高発現する CFPAC1 細胞を対象として、特異的 siRNA をトランスフェクションし、OEP1 結合蛋白群のリン酸化状態の変化について検討を行った。

C. 研究結果

I. CIM 結合分子の探索とその機能解析：

CIMを標的とするshort-hairpin RNA発現ベクターを用いて、高転移性LNM35細胞において、恒常的にCIMの発現を抑制する事により、顕著な細胞運動能・浸潤能の抑制が引き起こされる（図2左）。これは、我々が明らかとした、CIMの持つ、ERに局在しがん細胞が周囲の微小環境から絶えず受け続ける低酸素、或いは低栄養などのストレスに対する耐性を付与する機能（図2右）では説明がつかず、未知の機能の存在が示唆される。そこで、CIMの持つ細胞運動・浸潤能の制御機構の解明を目指して、CIM結合蛋白の探索を、プロテオミクス技術を

図２．CIM による運動・浸潤能と低酸素・小胞体ストレス耐性の付与

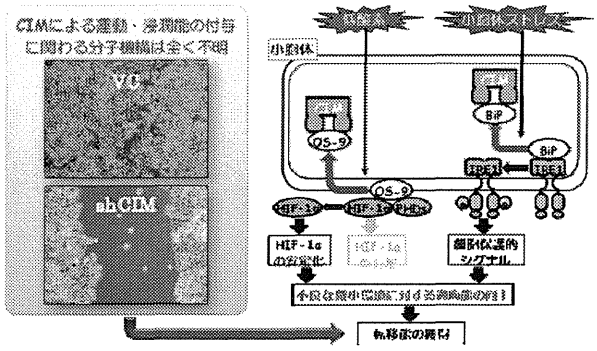

駆使する事により進めたところ、これまでに11種類の分子とCIMとの結合を確認している。本年度は、さらなる検証として、myc標識CIMを外来性にLNM35株で発現させ、抗myc抗体を用いたpull downを行い、共沈物に対してウェスタンブロット法を用いた解析を加えたところ、細胞内おけるCIMと候補４分子の結合が示唆される結果を得た。これらの分子の発現と肺がん臨床病態との関連について、我々が詳細な臨床情報とともに採取した７０例の肺腺癌腫瘍組織のマイクロアレイ解析データを用いて検討したところ、４種類の結合分子中の2分子において、高発現群が低発現群症例に比して有意に術後な予後を示した（図3左）。また、高転移性肺癌細胞亜株LNM35株が示す高い運動能と浸潤能は、これらの2分子のsiRNAを用いた発現抑制によって有意に減弱した（図3右）。

図３．CIM 結合分子の同定と、その機能的役割に関する検討

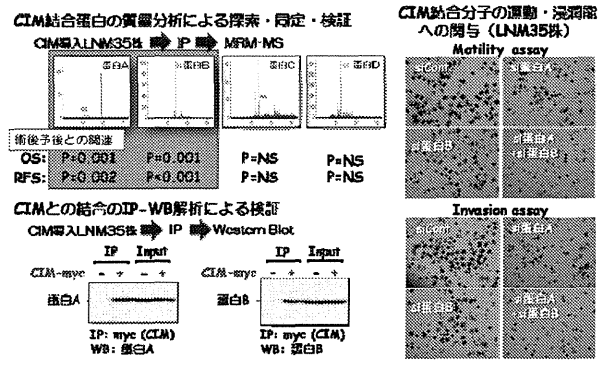

II. LNM35株のプロテオミクス解析による新規分子標的の探索・同定と応用：

LNM35 株という極めて有用なヒト肺がんの転移研究モデル系と、最新のプロテオミクス解析技術の両者を併せ持つ本研究グループの優位性を生かし、さらなる分子標的の探索・同定を並行して進めた。本年度は、プロテオミクス技術を駆使して、肺がんと同じく早期に転移をきたし極めて予後不良な代表的難治がんである膵臓がん組織と、肺がん転移研究モデル系における網羅的蛋白発現解析を進めた。膵臓がん組織において、正常主膵管と比較して 2 倍以上の発現差を認める蛋白を７種類同定し、さらには、LNM35 株において高発現の認められる蛋白として、OEP1 (Overexpressed in pancreatic cancer) と OEP2 を同定するに至った（図１左)。

膵臓がんと正常主膵管との比較において、OEP1 の発現差は OEP2 のそれより大きい事から、LNM35 並びに膵臓がん細胞株を用いて、転移能制御に関する OEP1 の機能解析を進めることとした。OEP1 を高発現する LNM35 株において、siRNA を用いた OEP1 の発現抑制は、がん細胞の運動能と浸潤能の両者を減弱させることが明らかとなった（図４左)。

一方、OEP1 低発現の膵がん細胞株 Panc-1 株に OEP1 を導入し安定発現細胞株を樹立し、細胞運動能、並びに浸潤能の変化に関する検討を行ったところ、いずれも OEP1 導入細胞株においてその亢進が認められた（図 4

右)。以上の結果より、OEP1 はがん細胞の転移能の制御に深く関与する事が示唆された。

図４．OEP1 の抑制或いは過剰発現によるがん細胞の運動・浸潤能の変化

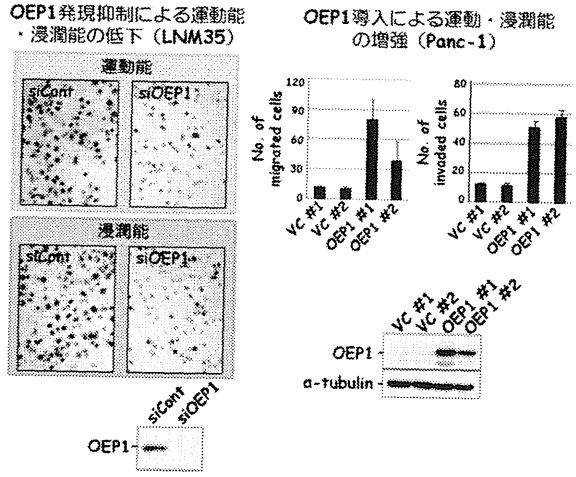

次に、OEP1 の機能について示唆を得るべく、OEP1 固相化カラムと質量分析装置を用いた結合蛋白の網羅的探索を行った結果、OEP1 結合蛋白候補 11 分子を同定するに至った（図 1 右)。これらの候補分子群のうち、解析系の不可避なノイズと考え得るヒストンとケラチンを除いた 9 分子について、OEP1 との結合に関する検証を行うべく、質量分析による精密蛋白定量法である MRM 解析を用いて解析を行った。その結果、細胞膜とアクチンを結合する ERM 蛋白の一つである Ezrin を含む 5 分子について、OEP1 との結合が確認された(図 1 右)。Ezrin は adhesion complex の構成分子として細胞接着性の制御に関わると共に、細胞内シグナル伝達においても重要な働きを担い細胞運動性の制御にも深く関わる事が知られている事から、OEP1 と Ezrin の制御関係についてさらなる検討を加えた。免疫沈降 - ウェスタンブロット法による結合の確認を進めた結果、膵臓がん細胞内における両分子の結合が確認された（図 5 左上)。

さらには、OEP1 の siRNA による発現抑制は、focal adhesion complex の形成不全と細胞接着性の減弱を惹起すると共に、c-Src による Ezrin のリン酸化を減弱させる事が明らかとなった（図 5 左下)。

図５．OEP1 の EZR との結合の同定と、その機能的役割の検討

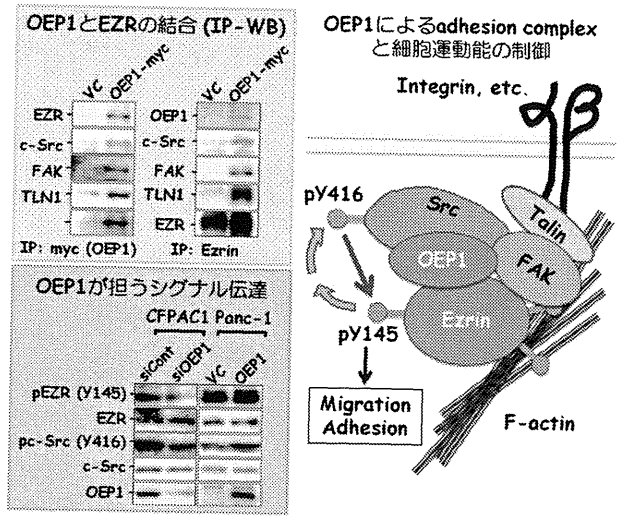

D. 考察及び結論

肺がんの浸潤・転移関連分子として同定した CIM について、プロテオミクス技術を応用した網羅的結合蛋白探索を進めた。同定した 2 種類の分子については、その発現と術後予後との間に有意な相関を認めるとともに、高転移性の LNM35 株における発現抑制がその細胞運動能・浸潤能を強く抑制することを見出した。これらの研究成果は、同定した２つの分子と CIM との結合が、CIM が付与する肺がん細胞の転移能の制御に関わっている可能性を強く示唆する。

また、LNM35 株と膵がん組織の両者の横断的なプロテオミクス解析によって進めたがん転移関連分子の探索は、OEP1 の同定につながった。本年度の研究成果は OEP1 が、が

ん細胞の運動・浸潤・転移に機能的に関与していることを示すとともに、その分子機序として、OEP1 の Ezrin との結合を通じた c-Src による Ezrin のリン酸化の促進と adhesion complex の安定化が関与している可能性が示唆された。

E. 研究発表

1. Hosono Y, Yamaguchi T, Mizutani E, Yanagisawa K, Arima C, Tomida S, Shimada Y, Hiraoka M, Kato S, Yokoi K, Suzuki M, Takahashi T: MYBPH, a transcriptional target of TTF-1, inhibits ROCK1, and reduces cell motility and metastasis. ***EMBO J*** 31: 481-493, 2012.
2. Yamaguchi T, Yanagisawa K, Sugiyama R, Hosono Y, ShimadaY, Arima C, Kato S, Tomida S, Suzuki M, Osada H, Takahashi T: NKX2-1/TITF1/TTF-1-induced ROR1 is required to sustain EGFR survival signaling in lung adenocarcinoma. ***Cancer Cell*** 21: 348-361, 2012.
3. Hosono Y, Usukura J, Yamaguchi T, Yanagisawa K, Suzuki M, Takahashi T: MYBPH inhibits NM IIA assembly via direct interaction with NMHC IIA and reduces cell motility. ***Biochem Biophys Res Commun*** 428 : 173-178, 2012.
4. Yanagisawa K, Tomida, S, Matsuo K, Arima C, Kusumegi M, Yokoyama Y, Ko SBH., Mizuno N, Kuroyanagi Y, Kwahara T, Takeuchi T, Goto H, Yamao K, Nagino M, Tajima K, Takahashi T: Seven-signal proteomic signature for detection of operable pancreatic cancer and their discrimination from autoimmune pancreatitis. ***Int. J. Proteomics***. 2012 (doi:10.1155/2012/510397).

F. 学会発表

1. Proteomic identification of potential biomarkers of malignant pulmonary mesothelioma. Kiyoshi Yanagisawa, Noriyasu Usami, Kenichiro Ono, Masashi Kondo,Tetsunori Hase, Seiichi Kato, Kasumi Yagi, Naoe Hotta, Shigeo Nakamura, Yoshinori Hasegawa, Kohei Yokoi ,Takashi Takahashi. 71st Annual Meeting of the Japanese Cancer Association (Symposia), Sapporo, September 19-21, 2012.
2. Quantitative Proteomic Profiling Identifies CKAP4 as a Malignant Pulmonary Mesothelioma-Associated Molecule that Regulates Metabolic Stress
   Kiyoshi Yanagisawa, Seiichi Kato, Naoe Hotta, Shigeo Nakamura,Takashi Takahashi.
   Cold Spring Harbor Meeting 2012 [Mechanisms&Models of Cancer] , 2012. Aug14-18, Cold Spring Harbor Labotaroty NY

G. 知的財産権の出願・登録状況

1. 特許出願
2. 実用新案登録
3. その他

いずれも、特記すべき事項無し

III. 研究成果の刊行に関する一覧表

研究成果の刊行に関する一覧

発表者氏名	論文タイトル名	発表誌名	巻号	ページ	出版年
Hosono Y, Yamaguchi T, Mizutani E, Yanagisawa K, Arima C, Tomida S, Shimada Y, Hiraoka M, Kato S, Yokoi K, Suzuki M, Takahashi T:	MYBPH, a transcriptional target of TTF-1, inhibits ROCK1, and reduces cell motility and metastasis.	EMBO J	31	481-493	2012
Yamaguchi T, Yanagisawa K, Sugiyama R, Hosono Y, ShimadaY, Arima C, Kato S, Tomida S, Suzuki M, Osada H, Takahashi T	NKX2-1/TITF1/TTF-1-induced ROR1 is required to sustain EGFR survival signaling in lung adenocarcinoma.	Cancer Cell	21	348-361	2012
Hosono Y, Usukura J, Yamaguchi T, Yanagisawa K, Suzuki M, Takahashi T	MYBPH inhibits NM IIA assembly via direct interaction with NMHC IIA and reduces cell motility.	Biochem Biophys Res Commun	428	173-178	2012
Yanagisawa K, Tomida, S, Matsuo K, Arima C, Kusumegi M, Yokoyama Y, Ko SBH., Mizuno N, Kuroyanagi Y, Kawahara T, Takeuchi T, Goto H, Yamao K, Nagino M, Tajima K, Takahashi T	Seven-signal proteomic signature for detection of operable pancreatic cancer and their discrimination from autoimmune pancreatitis.	Int J Proteomics		doi:10.1155/2012/510397	2012
Kalari S, Jung M, Kernstine KH, Takahashi T, Pfeifer GP	The DNA methylation landscape of small cell lung cancer suggests a differentiation defect of neuroendocrine cells.	Oncogene		doi: 10.1038/onc.2012.362	2012
Cao K, Tanaka K, Komizu Y, Tamiya-Koizumi K, Murate T, Ueoka R, Kyogashima M, Usukura J, Takahashi T, Suzuki M.	Hybrid liposomes affect cellular lipid constituents and caveolae structures.	Bioorg Med Chem Lett	22	1731-1733	2012

Endo M, Nakano M, Kadomatsu T, Fukuhara S, Kuroda H, Mikami S, Hato T, Aoi J, Horiguchi H, Miyata K, Odagiri H, Masuda T, Harada M, Horio H, Hishima T, Nomori H, Ito T Yamamoto Y, Minami T, Okada S, Takahashi T, Mochizuki N, Iwase H, Oike Y	Tumor cell-derived angiopoientin-like protein 2 in metastasis.	Cancer Res	72	1784-1794	2012
Akatsuka S, Yamashita Y, Ohara H, Liu Y-T, Izumiya M, Abe K, Ochiai M, Jiang L, Nagai H, Okazaki Y, Murakami H, Sekido Y, Arai E, Kanai Y, Hino O, Takahahi T, Nakagama H, Toyokuni S	Fenton reaction induced cancer in wild type rats recapitulates genomics alterations observed in human cancer.	PLoS ONE		e43403. doi:10.1371/journal.pone.0043403	2012
Jiang L Akatsuka S, Nagai H, Chew S-H, Ohara H, Okazaki Y, Yamashita Y, Yoshikawa Y, Yasui H, Ikuta K, Sasaki K, Kohgo Y, Hirano S, Shinohara Y, Kohyama N, Takahashi T, Toyokuni S	Iron overload signature in chrysotile-induced malignant mesothelioma.	J Pathol	228	366-377	2012
Fujii M, Toyoda T, Nakanishi H, Yatabe Y, Sato A, Matsudaira Y, Ito H, Murakami H, Kondo Y, Kondo E, Hida T, Tsujimura T, Osada H, Sekido Y	TGF-β synergizes with defects in the Hippo pathway to stimulate human malignant mesothelioma growth.	J Exp Med	209	479-494	2012
Mizuno T, Murakami H, Fujii M, Ishiguro F, Tanaka I, Kondo Y, Akatsuka S, Toyokuni S, Yokoi K, Osada H, Sekido Y	YAP induces malignant mesothelioma cell proliferation by upregulating transcription of cell cycle promoting genes.	Oncogene	31	5117-5122	2012
Shinjo K, Okamoto Y, An B, Yokoyama T, Takeuchi I, Fujii M, Osada H, Usami U, Hasegawa Y, Ito H, Hida T, Fujimoto N, Kishimoto T, Sekido S, Kondo Y	Integrated analysis of genetic and epigenetic alterations reveals CpG island methylator phenotype associated with distinct clinical	Carcinogenesis	33	1277-1285	2012

	characters of lung adenocarcinoma.				
Katsushima K, Shinjo K, Natsume A, Ohka F, Fujii F, Osada H, Sekido Y, Kondo Y	Contribution of microRNA-1275 to Claudin11 protein suppression via polycomb-mediated silencing mechanism in human glioma stem-like cells.	J Biol Chem	287	27396-27406	2012
Attoub S, Sperandio O, Raza H, Arafat K, Al-Salam S, Al Sultan MA, Al Safi M, Takahashi T, Adem A	Thymoquinone as an anticancer agent: evidence from inhibition of cancer cells viability and invasion in vitro and tumor growth in vivo.	Fundam Clin Pharmacol		doi: 10.1111/j.1472-8206.2012.01056.x.	2012
Attoub S, Arafat K, Gelaude A, Sultan MAA, Bracke M, Collin, P, Takahashi T, Adrian, T, De Wever O: Frondoside	A suppressive effects on lung cancer survival, tumor growth, angiogenesis, invasion, and metastasis.	PLoS ONE		doi: 10.1371/journal.pone.0053087.	2013
Suda K, Tomizawa K, Osada H, Maehara Y, Yatabe Y, Sekido Y, Mitsudomi T	Conversion from the "oncogene addiction" to "drug addiction" by intensive inhibition of the EGFR and MET in lung cancer with activating EGFR mutation.	Lung Cancer	76	292-299	2012
Ishiguro F, Murakami H, Mizuno T, Fujii M, Kondo Y, Usami N, Yokoi K, Osada H, Sekido Y	Activated Leukocyte Cell Adhesion Molecule (ALCAM) Promotes Malignant Phenotypes of Malignant Mesothelioma.	J Thorac Oncol	7	890-899	2012
Elshazley M, Sato M, Hase T, Takeyama Y, Yamashita R, Yoshida K, Toyokuni S, Ishiguro F, Osada H, Sekido Y, Yokoi K, Usami N, Shames DS, Kondo M, Gazdar AF, Minna JD, Hasegawa Y	The circadian clock gene BMAL1 is a novel therapeutic target for malignant mesothelioma.	Int J Cancer	131	2820-31	2012

IV. 研究成果の刊行物・別刷

The EMBO Journal (2012) 31, 481–493 | © 2012 European Molecular Biology Organization | All Rights Reserved 0261-4189/12
www.embojournal.org

THE EMBO JOURNAL

MYBPH, a transcriptional target of TTF-1, inhibits ROCK1, and reduces cell motility and metastasis

Yasuyuki Hosono[1,2], Tomoya Yamaguchi[1], Eri Mizutani[1], Kiyoshi Yanagisawa[1,3], Chinatsu Arima[1], Shuta Tomida[1], Yukako Shimada[1], Michiyo Hiraoka[1], Seiichi Kato[1], Kohei Yokoi[2], Motoshi Suzuki[1] and Takashi Takahashi[1,*]

[1]Division of Molecular Carcinogenesis, Center for Neurological Diseases and Cancer, Nagoya University Graduate School of Medicine, Nagoya, Japan, [2]Department of Thoracic Surgery, Nagoya University Graduate School of Medicine, Nagoya, Japan and [3]Institute for Advanced Research, Nagoya University, Nagoya, Japan

Cell migration driven by actomyosin filament assembly is a critical step in tumour invasion and metastasis. Herein, we report identification of *myosin binding protein H* (*MYBPH*) as a transcriptional target of *TTF-1* (also known as *NKX2-1 and TITF1*), a master regulator of lung development that also plays a role as a lineage-survival oncogene in lung adenocarcinoma development. MYBPH inhibited assembly competence-conferring phosphorylation of the myosin regulatory light chain (RLC) as well as activating phosphorylation of LIM domain kinase (LIMK), unexpectedly through its direct physical interaction with Rho kinase 1 (ROCK1) rather than with RLC. Consequently, MYBPH inhibited ROCK1 and negatively regulated actomyosin organization, which in turn reduced single cell motility and increased collective cell migration, resulting in decreased cancer invasion and metastasis. Finally, we also show that *MYBPH* is epigenetically inactivated by promoter DNA methylation in a fraction of *TTF-1*-positive lung adenocarcinomas, which appears to be in accordance with its deleterious functions in lung adenocarcinoma invasion and metastasis, as well as with the paradoxical association of *TTF-1* expression with favourable prognosis in lung adenocarcinoma patients.

The EMBO Journal (2012) **31**, 481–493. doi:10.1038/emboj.2011.416; Published online 15 November 2011
Subject Categories: cell & tissue architecture
Keywords: actomyosin; cytoskeleton; lung cancer; ROCK1

Introduction

Metastasis is thought to be initiated by disruption of cell–cell contact, followed by single cell migration. It is widely accepted that contractile motion of cancer cells is generated by assembly and consecutive contraction of actomyosin bundles (Lauffenburger and Horwitz, 1996; Friedl and Wolf, 2003; Hall, 2009). Collective cell migration has been shown to result from decreasing actomyosin contractility at the sites of cell–cell contact and plays a role in a range of developmental processes as well as cancer invasion (Christiansen and Rajasekaran, 2006; Hidalgo-Carcedo *et al*, 2011).

Non-muscle myosin II (NM II), a major component of the actomyosin cytoskeleton, comprising two non-muscle myosin heavy chains (NMHCs) and two essential myosin light chains (ELCs), as well as two regulatory light chains (RLCs) (Conti and Adelstein, 2008; Vicente-Manzanares *et al*, 2009). Emerging evidence indicates that NM II members, especially NM IIA, are crucially involved in cancer cell migration, invasion, and metastasis via bivalent binding to actin filaments (Betapudi *et al*, 2006; Huang *et al*, 2009; Medjkane *et al*, 2009). Rho kinase 1 (ROCK1), a downstream effecter of RhoA, is a major positive regulator of that process, which is thought to be executed through phosphorylation of RLC and subsequent unfolding of NM IIA into an assembly competent form capable of NM IIA dimer formation. In addition, ROCK1 phosphorylates LIM domain kinase (LIMK) and stabilizes actin filaments through inactivation of the actin-depolymerizing factor cofilin. Another member of the ROCK family, ROCK2, is abundantly and preferentially expressed in non-epithelial tissues such as the brain and muscles, and plays roles in phagocytosis and cell contraction (Etienne-Manneville and Hall, 2002; Riento and Ridley, 2003; Amano *et al*, 2010). However, how actomyosin organization in non-muscle cells is negatively regulated to counterbalance the positive regulatory function of ROCK1 largely remains to be elucidated.

TTF-1 is a lineage-specific transcription factor required for branching morphogenesis and physiological lung functions (Kimura *et al*, 1996). TTF-1 is also involved in pathological conditions of the lung. For example, TTF-1 expression is prominent in lung epithelial cells undergoing regeneration (White *et al*, 2001; Pogach *et al*, 2007). A major fraction of lung adenocarcinomas are also TTF-1 positive, which is suggested to reflect their derivation from the terminal respiratory unit (Yatabe *et al*, 2002; Takeuchi *et al*, 2006). We and others recently identified TTF-1 as a lineage-survival oncogene with focal amplification in lung adenocarcinomas (Kendall *et al*, 2007; Tanaka *et al*, 2007; Weir *et al*, 2007; Kwei *et al*, 2008). However, it is of note that *TTF-1* expression is associated with favourable prognosis in lung adenocarcinoma cases (Anagnostou *et al*, 2009). In the present study, we identified MYBPH as a transcriptional target of TTF-1, which provides a clue for elucidating the molecular mechanism related to how TTF-1 paradoxically inhibits cancer invasion and metastasis.

Results

MYBPH is directly transactivated by TTF-1

As an initial step towards a better understanding of transcriptomes regulated by *TTF-1*, microarray analysis was

*Corresponding author. Division of Molecular Carcinogenesis, Center for Neurological Diseases and Cancer, Nagoya University Graduate School of Medicine, 65 Tsurumai, Showa-ku, Nagoya 466-8550, Japan. Tel.: +81 52 744 2454; Fax: +81 52 744 2457;
E-mail: tak@med.nagoya-u.ac.jp

Received: 28 May 2011; accepted: 18 October 2011; published online: 15 November 2011

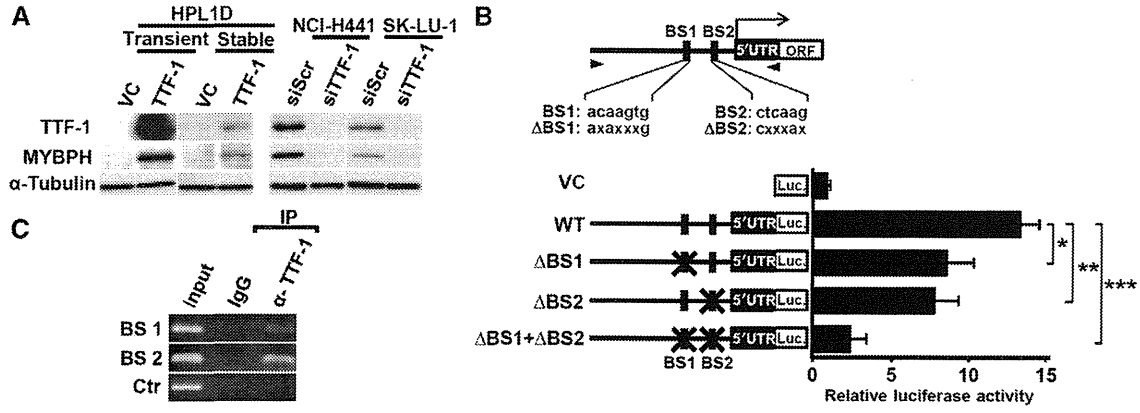

Figure 1 *MYBPH* is directly transactivated by TTF-1. (**A**) Western blot analysis showing induction of MYBPH in HPL1D cells transiently or stably transfected with TTF-1, as well as reduction by TTF-1 knockdown in NCI-H441 and SK-LU-1 cells. siScr, negative control siRNA; siTTF-1, siRNA against TTF-1. (**B**) Top panel: schematic diagram of *MYBPH* promoter region, BS1 and BS2, putative NKX2-5 and TTF-1 binding sites, respectively. Arrowheads, locations of primers used to amplify *MYBPH* promoter. Bottom panel: luciferase reporter analysis using HPL1D cells with transient TTF-1-expression. Three independent experiments were performed in triplicate. Bars, mean ± s.d.; $*P<0.05$; $**P<0.01$; $***P<0.005$. (**C**) Chromatin immunoprecipitation assay of NCI-H441 cells showing that TTF-1 protein binds to both BS1 and BS2. Figure source data can be found with the Supplementary data.

performed using an immortalized peripheral lung epithelial cell line, HPL1D (Masuda *et al*, 1997), which was transiently transfected with *TTF-1*. We consequently identified *MYBPH* as the most highly upregulated gene (Supplementary Figure S1) and confirmed its upregulation at the protein level by western blot analysis (Figure 1A). A dual-luciferase assay also revealed *TTF-1*-mediated transcriptional activation of *MYBPH* (Figure 1B; Supplementary Figure S2A), while a chromatin immunoprecipitation (ChIP) assay of NCI-H441 cells clearly demonstrated specific binding of TTF-1 with both potential TTF-1 binding sites in the *MYBPH* promoter (Figure 1C).

MYBPH expression is inactivated by the promoter CpG methylation

TTF-1 was invariably present in lung adenocarcinoma cell lines expressing MYBPH at readily detectable levels (Figure 2A), while a significant correlation between TTF-1 and MYBPH expression was also observed in the analysis of our previous microarray data set of 90 lung adenocarcinoma cases ($P=0.0051$; Figure 2B; Takeuchi *et al*, 2006). Interestingly, however, we noted that a considerable fraction of lung adenocarcinomas both *in vitro* and *in vivo* expressed low levels of *MYBPH* despite high *TTF-1* expression. Therefore, we evaluated whether aberrant DNA methylation of the *MYBPH* promoter was involved in silencing of *MYBPH*. Treatment with a DNA demethylating agent, 5-Aza-dC, significantly induced *MYBPH* in NCI-H358 and A427 cells (Figure 2C), while bisulphite sequencing analysis revealed clear distinctions in terms of dense DNA methylation surrounding the genuine TTF-1 binding site (BS2; Li *et al*, 1998), but not that for the TTF-1 homologue, NKX2-5 (BS1; Chen and Schwartz, 1995), in NCI-H358 and A427 cells (Figure 2D; Supplementary Figure S2B). Methylation-specific PCR (MSP) analysis using DNA from laser microdissected specimens further confirmed the presence of aberrant DNA methylation specifically in *MYBPH*$^-$/*TTF-1*$^+$ lung adenocarcinoma tissues *in vivo* (Figure 2E). The present findings thus indicate that *MYBPH* is a direct transcriptional target of *TTF-1*, which is inactivated by promoter DNA methylation in a considerable fraction of lung adenocarcinomas.

MYBPH reduces cell motility, invasion, and metastasis

NM II is a major component of the actomyosin cytoskeleton in non-muscle cells and crucially involved in cell migration (Betapudi *et al*, 2006; Conti and Adelstein, 2008; Huang *et al*, 2009; Medjkane *et al*, 2009; Vicente-Manzanares *et al*, 2009). The presence of inactivating promoter DNA methylation led us to speculate that *TTF-1*-induced *MYBPH* might play a negative regulatory role in cell motility. Indeed, we found that treatment with small interfering RNA (siRNA) against *MYBPH* (siMYBPH) markedly increased the motility of NCI-H441 cells. Conversely, overexpression of MYBPH reduced Madin-Darby canine kidney (MDCK) cell motility (Figure 3A; Supplementary Figure S3), while that negative effect was cancelled by simultaneous treatment with siMYBPH (Supplementary Figure S4). Similarly, acquisition of the motile phenotype in siMYBPH-treated NCI-H441 cells was clearly demonstrated by results of a scratch assay (Figure 3B) as well as those of a Matrigel invasion assay (Figure 3C), with opposite effects observed in MYBPH-overexpressing MDCK cells. Next, we employed a three-dimensional Matrigel invasion assay and found that MYBPH-overexpressing MDCK cells invaded over a shorter distance and in a more collective manner than the control cells (Figure 3D). Neither siMYBPH treatment of NCI-H441 cells nor forced MYBPH overexpression in MDCK cells had an effect on cell growth (Supplementary Figure S5). We also noted that overexpression of TTF-1 reduced cell motility in HPL1D cells, which was significantly reverted by siMYBPH treatment (Figure 3E), supporting the notion that TTF-1-induced MYBPH negatively affects cell motility.

We also evaluated the effects of MYBPH expression on metastasis using a highly metastatic MYBPH-negative lung cancer cell line, NCI-H460-LNM35 (Kozaki *et al*, 2000). Stable transfectants expressing MYBPH at a level comparable to that in lung adenocarcinoma cell lines (Figure 4A) exhibited significantly reduced lung metastasis (Figure 4B and C), without affecting primary tumour growth (Supplementary Figure S6). Conversely, siMYBPH-treated NCI-H441 cells exhibited increased experimental lung metastasis (Figure 4D and E). In line with the present experimental findings, it was noted that decreased *MYBPH* expression was significantly

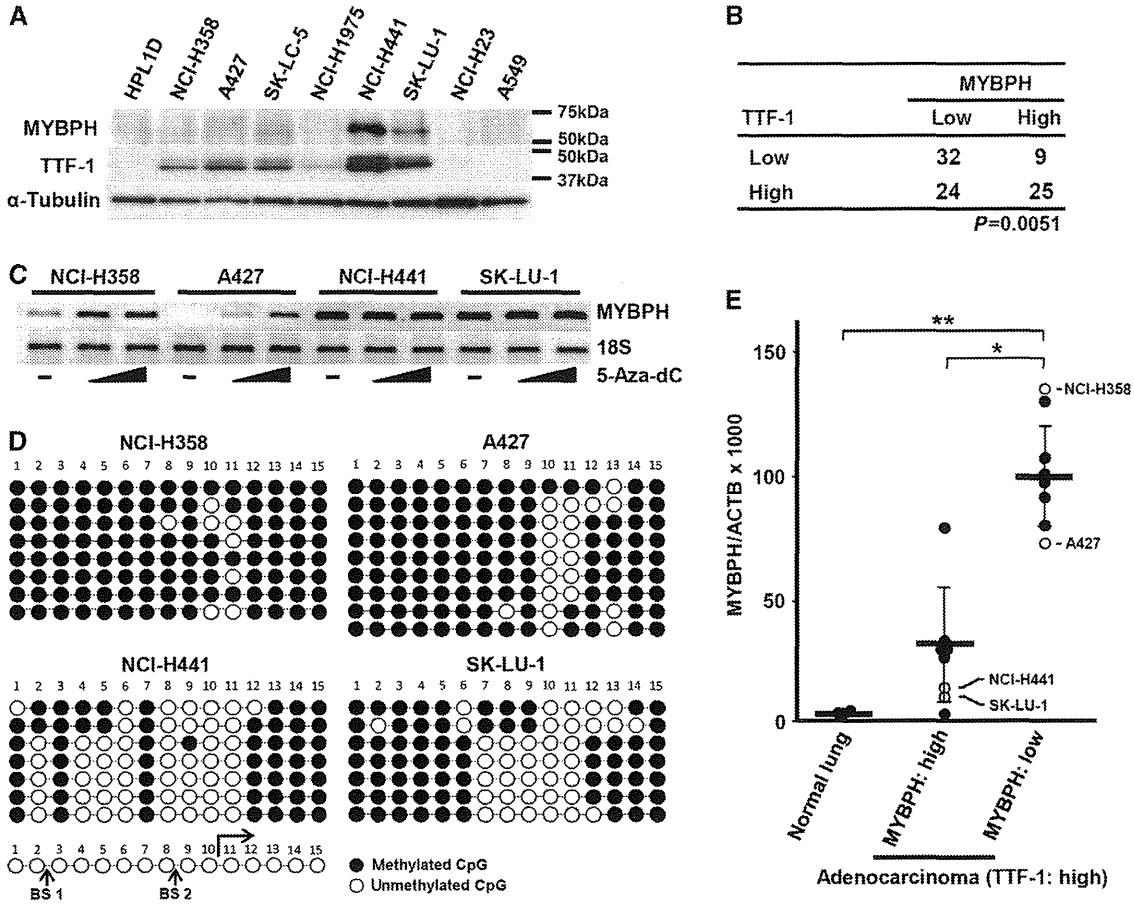

Figure 2 MYBPH expression is inactivated by the promoter CpG methylation. (**A**) Western blot analysis of MYBPH and TTF-1 in lung adenocarcinoma cell lines. (**B**) Correlation between *TTF-1* and *MYBPH* expressions in 90 lung adenocarcinoma specimens. Cases were classified into those above or below the average level of expression. (**C**) Semiquantitative RT–PCR analysis of four cell lines showing *MYBPH* induction in TTF-1-1$^+$/MYBPH$^-$-NCI-H358 and A427 cells after treatment with 5-Aza-dC. 18S served as a loading control. (**D**) Bisulphite sequencing analysis showing dense DNA methylation around BS2 in TTF-1$^+$/MYBPH$^-$-NCI-H358 and A427 cells. (**E**) Methylation-specific PCR analysis of the eighth CpG site in (**D**) using DNA from laser microdissected specimens and representative cell lines, which revealed aberrant DNA methylation in TTF-1$^+$/MYBPH$^-$ lung adenocarcinoma tissues and cell lines. Six cases each of MYBPH-positive and -negative lung adenocarcinomas with abundant TTF-1 expression, along with three normal lung tissues were analysed. Solid circles, clinical samples; open circles, cell lines; bars, mean ± s.d.; $^*P<0.001$; $^{**}P<0.0001$. Figure source data can be found with the Supplementary data.

associated with more apparent invasiveness in surgical specimens obtained from the 90 human lung adenocarcinoma cases (Figure 4F).

MYBPH affects actomyosin organization and cell morphology

We also found that siMYBPH treatment markedly altered the shape of the cells, as they showed a rounded morphology or occasionally bleb-like structures characterized by the appearance of peripheral actomyosin bundles, with clear colocalization of NMHC IIA with the peripheral actin bundles (Figure 5A; Supplementary Figure S7, left). Conversely, overexpression of MYBPH disrupted actomyosin organization as well as the normal morphology in MDCK cells (Figure 5B; Supplementary Figure S7, right). Taken together, these findings strongly support the notion that MYBPH is involved in the regulation of cell shape, motility, invasion, and metastasis.

MYBPH inhibits phosphorylation of RLC through interaction with ROCK1

Our findings strongly suggested that MYBPH is involved in actin organization. We, therefore, analysed changes in the proportion of triton-insoluble F-actin (TIF), a crosslinked meshwork of actin filaments that includes stress fibers (Watts and Howard, 1992), in relation to the level of MYBPH expression. We observed that siMYBPH-treated NCI-H441 cells contained a larger proportion of TIF pools than those treated with the siRNA control. In contrast, *MYBPH*-introduced MDCK cells contained fewer TIF pools than the control cells (Figure 6A).

Phosphorylation of RLC unfolds assembly incompetent NM IIA into assembly competent NM IIA, which is a prerequisite for its assembly and subsequent actomyosin reorganization (Conti and Adelstein, 2008; Vicente-Manzanares *et al*, 2009). In this connection, we found that NCI-H441 knocked down for *MYBPH* exhibited increased RLC phosphorylation, whereas introduction of *MYBPH* reduced the RLC phosphorylation level in MDCK cells (Figure 6B). This finding prompted us to investigate whether MYBPH is involved in the regulation of ROCK-mediated phosphorylation of RLC, since ROCK1 and 2 have been shown to play a central role in the regulation of RLC phosphorylation as downstream effectors of RhoA (Conti and Adelstein, 2008; Vicente-Manzanares *et al*, 2009). *In-vitro* protein–protein binding

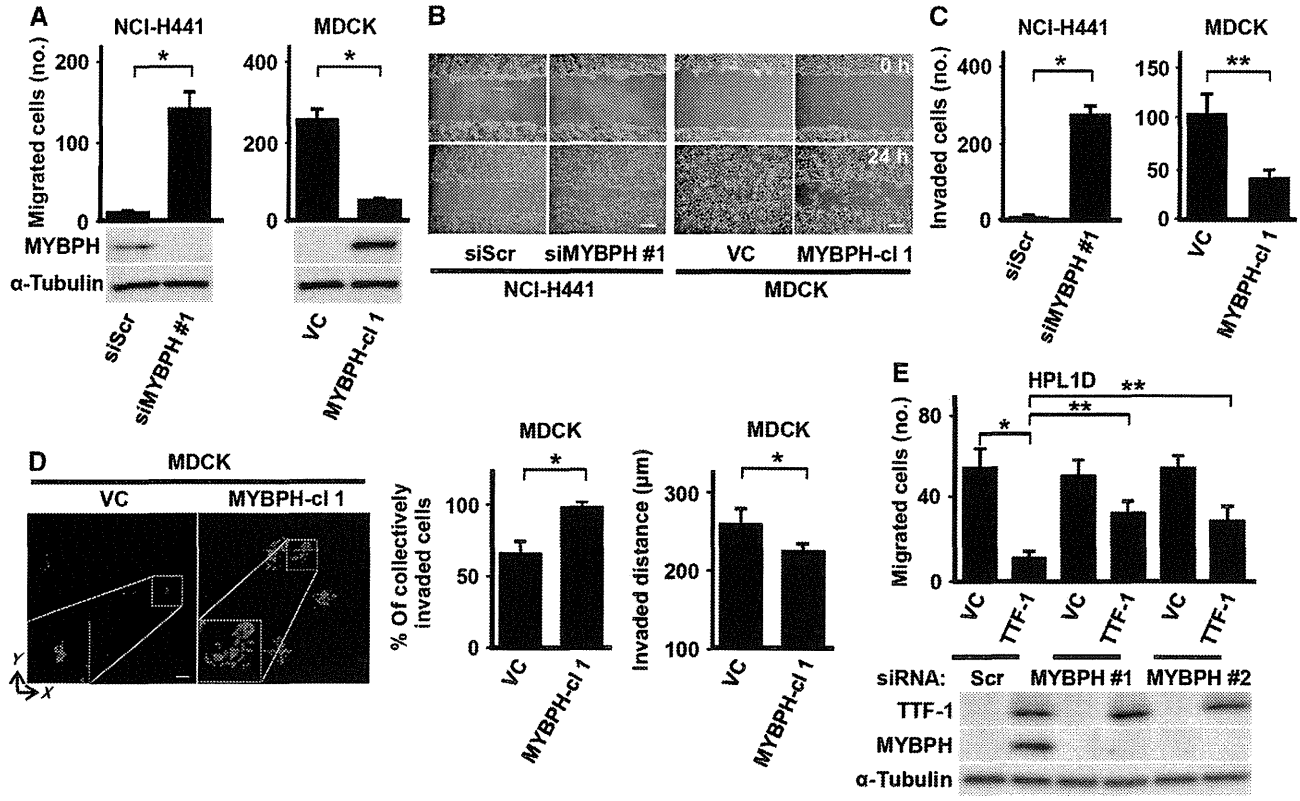

Figure 3 MYBPH reduces cell motility and invasion *in vitro*, and increases collective cell migration. (**A**) Motility assay showing increased *in-vitro* motility by MYBPH knockdown in NCI-H441 cells as well as reduced motility in stable MYBPH transfectant of MDCK cells. Three independent experiments were performed in triplicate. siMYBPH, siRNA against MYBPH; MYBPH-cl 1, MYBPH-transfected clone; bars, mean ± s.d.; $*P<0.01$. Results of corresponding western blot analysis of MYBPH are shown below. (**B**) Scratch assay showing increased *in-vitro* motility by MYBPH knockdown in NCI-H441 cells as well as reduced motility in stable MYBPH transfectant of MDCK cells. Photographs were taken at 24 h after scratch injury. Bars indicate 200 μm. (**C**) Matrigel invasion assay showing increased *in-vitro* invasion by MYBPH knockdown in NCI-H441 cells as well as reduced invasion in stable MYBPH transfectant of MDCK cells. Three independent experiments were performed in triplicate. Bars, mean ± s.d.; $*P<0.001$; $**P<0.01$. (**D**) Three-dimensional Matrigel invasion assay showing collective cell migration and decreased *in-vitro* invasion in stable MYBPH transfectant of MDCK cells. The proportions of cells with collective invasion were evaluated as described in Materials and methods. Data shown represent four independent experiments each counting > 100 cells. White bars indicate 50 μm. Bars, mean ± s.d.; $*P<0.001$. (**E**) Motility assay findings showing reduced *in-vitro* motility in stable TTF-1 transfectants of HPL1D cells, which was cancelled by treatment with siMYBPH. Three independent experiments were performed in triplicate. Bars, mean ± s.d.; $*P<0.01$; $**P<0.05$. The results of corresponding western blot analyses of TTF-1 and MYBPH are shown below. Figure source data can be found with the Supplementary data.

assays were performed to examine whether MYBPH directly interacts with RLC and/or ROCK1 and 2, using a purified His-tagged MYBPH protein with either purified GST-tagged ROCK1, ROCK2, or RLC proteins. Consequently, a direct interaction of MYBPH specifically with ROCK1, but not with RLC, was unexpectedly revealed (Figure 6C). *In-vitro* ROCK kinase assays using purified ROCK1, ROCK2, and RLC proteins in the presence or absence of purified MYBPH protein demonstrated inhibition of ROCK1-mediated RLC phosphorylation by inclusion of MYBPH in the reaction mixture, whereas the presence of MYBPH had no effects on ROCK2-mediated RLC phosphorylation *in vitro*, consistent with the *in-vitro* binding assay results (Figure 6D; Supplementary Figure S8). We also noted that MYBPH was not phosphorylated by either ROCK1 or ROCK2 (Supplementary Figure S8). Immunoprecipitation–western blot (IP–WB) analysis also showed an association of MYBPH with ROCK1 in MYBPH-overexpressing MDCK and NCI-H441 cells, respectively (Figure 6E; Supplementary Figure S9). Overexpression of MYBPH reduced the interaction between ROCK1 and RLC in MDCK, whereas siMYBPH treatment increased their interaction in NCI-H441 cells (Figure 6F). In contrast, the interaction between RhoA and ROCK1 was not affected by MYBPH (Supplementary Figure S10), which appears to be consistent with the interaction of MYBPH with purified GST-tagged ROCK1 protein lacking a RhoA-binding domain near the C-terminus. In addition, IP–WB analysis showed lack of interactions of MYBPH with various RLC kinases (Supplementary Figure S11), including myosin light chain kinase (MLCK), myotonic dystrophy kinase-related CDC42 binding protein kinase alpha and beta (MRCKα and β), citron, and Zipper interacting protein kinase (ZIPK) (Matsumura, 2005).

Further analysis using various deletion mutants of MYBPH showed that the fibronectin type III domain of MYBPH was required for MYBPH binding to ROCK1 (Figure 7A; Supplementary Figure S12). Consistently, a deletion mutant devoid of the fibronectin type III domain did not elicit MYBPH overexpression-induced alterations in cell morphology and actomyosin bundle formation or decreased cell motility in MDCK cells (Figure 7B; Supplementary Figure S13). We also found that MYBPH affects the phosphorylation state of LIMK and cofilin (Figure 7C), which are known to participate in the cascade downstream of ROCK1, thus regulating actin polymerization (Maekawa *et al*, 1999; Yoshioka

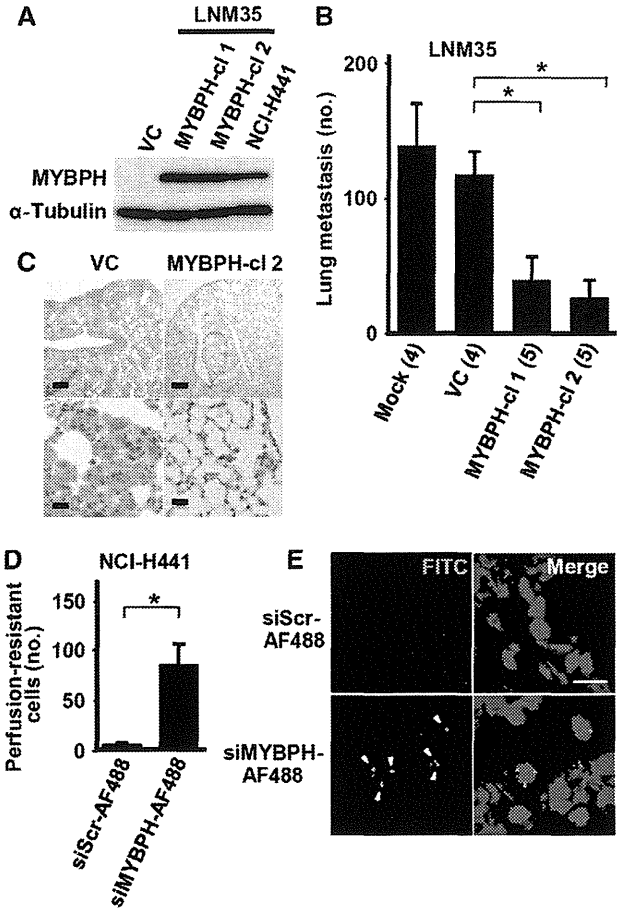

F

Invasion	MYBPH Low	MYBPH High
Definite	46	19
Definite but focal	8	7
Negligible/Negative	2	8

P=0.0065

Figure 4 MYBPH reduces invasion and metastasis *in vivo*. (**A**) Western blot analysis showing expression levels of MYBPH in stable transfectants of NCI-H460-LNM35 (LNM35-MYBPH-cl 1 and -cl 2) expressing MYBPH at a level comparable to that in NCI-H441. (**B**) Decreased lung metastasis in stable MYBPH transfectants of LNM35. Forty days after subcutaneous inoculation, lung metastases were counted. Bars, mean ± s.d.; $*P<0.01$. Numbers in parentheses indicate inoculated mice. (**C**) Representative haematoxylin and eosin-stained images of lung metastases. Bars indicate 200 μm in upper and 20 μm in lower panels. (**D**) Experimental metastasis assay of NCI-H441 cells knocked down for MYBPH with Alexa Fluor 488-conjugated siMYBPH #1 (siMYBPH #1-AF488) (five mice per treatment). Bars, mean ± s.d.; $*P<0.001$. (**E**) Representative fluorescence images of perfusion-resistant cells. Cells were also stained with DAPI (blue). Bars indicate 10 μm. (**F**) Relationships between *MYBPH* expression and invasion status in our previously reported microarray data set of human lung adenocarcinomas. Cases were classified into those above and below the average level of expression. Figure source data can be found with the Supplementary data.

et al, 2003). Consistent with the present findings, increased motility, RLC phosphorylation, and organization of peripheral actomyosin bundles induced by MYBPH knockdown in NCI-H441 cells were significantly, though not completely, counteracted by simultaneous treatment with the ROCK-specific inhibitor Y-27632 (Figure 7D; Supplementary Figure S14). It was also found that increased cell motility and RLC phosphorylation induced by siMYBPH treatment were counteracted by simultaneous treatment with siROCK1, but not with siROCK2 (Figure 7E). Thus, it was demonstrated that MYBPH binds to ROCK1 but not to RLC, leading to inhibition of ROCK1-mediated regulation of actomyosin organization including assembly competence-conferring RLC phosphorylation and activation of the LIMK–cofilin pathway.

MYBPH increases cell–cell contact and collective cell migration

A decrease in ROCK-driven actomyosin contractility enhances cell–cell contact and collective cancer cell invasion (Sahai and Marshall, 2002; Hidalgo-Carcedo *et al*, 2011). Along this line, NCI-H441 cells knocked down for MYBPH migrated mostly as single cells in a three-dimensional invasion assay, which was reverted by simultaneous treatment with Y-27632 (Figure 8A). This siMYBPH-mediated increase in single cell migration was markedly counteracted by simultaneous treatment with siROCK1 (Figure 8B). While one of the hallmarks characterizing collective cell migration is preservation of the integrity of cell–cell contact during movement (Friedl and Gilmour, 2009), MYBPH knockdown markedly decreased cell–cell contact in NCI-H441 cells, as shown in our aggregation assay. This effect was clearly counteracted by a simultaneous treatment with Y-27632 (Figure 8C). Conversely, overexpression of MYBPH reduced MDCK cell aggregation (Figure 8D). Formation of adherence junctions positively regulate cell–cell contacts in epithelial cells (Friedl and Wolf, 2010). Our aggregation assay findings showed that siMYBPH-treated NCI-H441 cells exhibited a readily detectable decrease in E-cadherin staining intensity on the cell surface, which was considerably counteracted by simultaneous treatment with Y-27632 (Figure 8E). Conversely, overexpression of MYBPH increased E-cadherin intensity in MDCK cells similarly examined by an aggregation assay (Supplementary Figure S15). Interestingly, western blot analysis demonstrated similar levels of E-cadherin expression irrespective of MYBPH state. Taken together, the present findings indicate that TTF-1-inducible MYBPH inhibits ROCK1 through direct interaction, which in turn negatively regulates actomyosin organization, leading to decreased cell motility, invasion, and metastasis (Figure 9).

Discussion

The present findings indicate that *MYBPH*, which we identified here as a direct transcriptional target of *TTF-1*, plays multiple roles in negative regulation of actomyosin organization. Among the various myosin binding proteins, a cardiac isoform of *MYBPC* (*cMYBPC*) has been the focus of intense research activities, because of its direct involvement in cardiovascular diseases such as familial hypertrophic cardiomyopathy (Bonne *et al*, 1995; Watkins *et al*, 1995; Richard *et al*, 2003). While *MYBPH* and *cMYBPC* possess significant homology at their carboxyl termini, *MYBPH* lacks a region homologous to the amino terminal half of *cMYBPC*, which is required for inhibition of myosin functions. To date, very little is known about the functions of *MYBPH*, even in regard to its interaction with muscle myosin (Yamamoto, 1988; Welikson and Fischman, 2002), with virtually nothing reported regarding its roles in non-muscle cells.

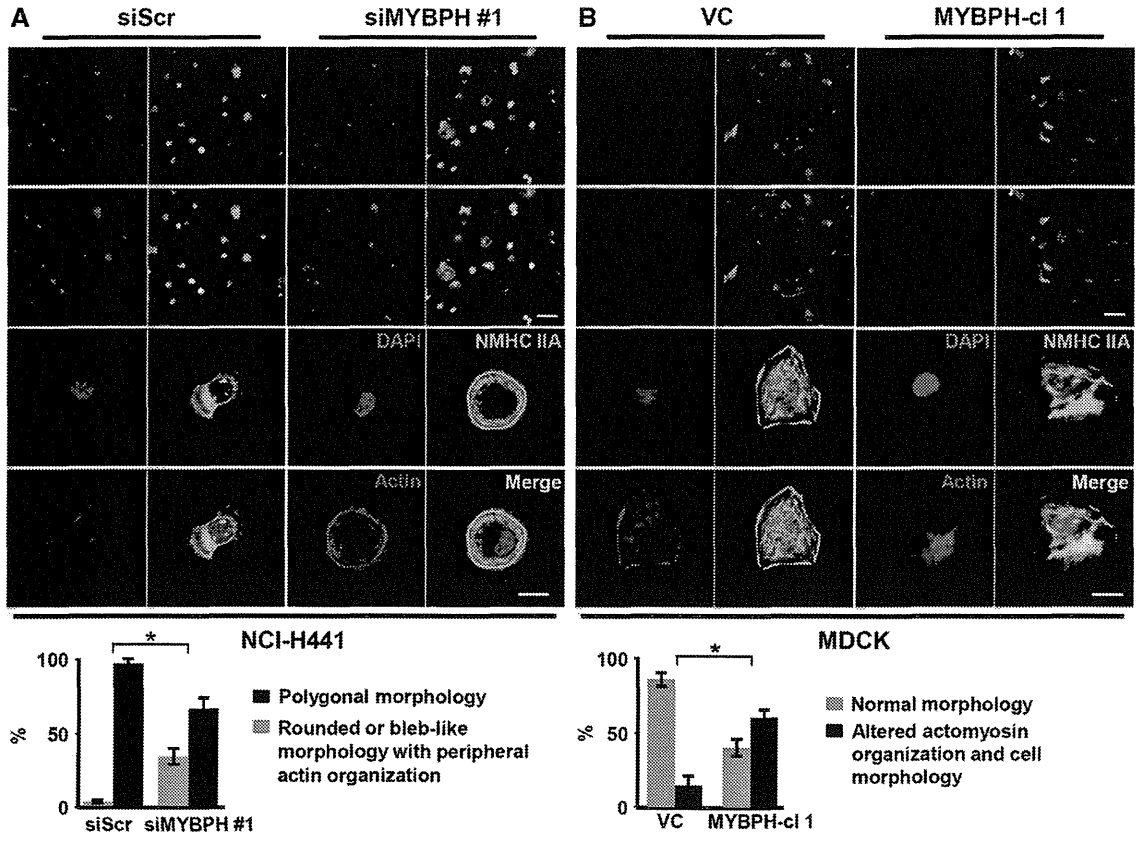

Figure 5 MYBPH affects actomyosin organization and cell morphology. (**A**) Top panels: immunofluorescence staining for DAPI (blue), actin (red), and NMHC IIA (green) in NCI-H441 cells treated with siScr or siMYBPH. Bars indicate 100 μm in top and 10 μm in bottom panels. Bottom panel: proportions of cells according to morphology. Data shown represent three independent experiments each counting >100 cells. Bars, mean ± s.d.; $^*P<0.001$. Results with an additional siMYBPH are also shown in the left panels of Supplementary Figure S7. (**B**) Top panels: immunofluorescence staining for DAPI (blue), actin (red), and NMHC IIA (green) in MDCK cells stably transfected with empty or MYBPH-expressing vectors. Bars indicate 100 μm in top and 10 μm in bottom panels. Bottom panel: proportions of cells according to morphology, which were determined as shown in (**A**). Bars, mean ± s.d.; $^*P<0.001$. Results obtained with an additional independent clone are shown in the right panels of Supplementary Figure S7.

In this study, we found that MYBPH inhibits assembly competence-conferring RLC phosphorylation as well as activating phosphorylation of LIMK. MYBPH unexpectedly executes such inhibitory activities by direct physical interaction with ROCK1 rather than with RLC, which results in inhibition of ROCK1 kinase activity. ROCK1 is a downstream effector of RhoA that is crucially involved in cell morphogenesis and motility, as well as in cancer progression (Itoh *et al*, 1999; Sahai and Marshall, 2003; Wilkinson *et al*, 2005; Wong *et al*, 2008). To date, however, very few examples have been reported as negative regulators of ROCK1. While RhoE has been shown to inhibit ROCK1 by competing with RhoA for ROCK1 (Riento *et al*, 2003), MYBPH directly binds to and interferes with ROCK1, which in turn inhibits RLC phosphorylation. Our findings thus add MYBPH to the small list of negative ROCK1 regulators, suggesting a complex nature of the negative regulatory mechanisms of ROCK1.

It is interesting that marked distinctions were observed in terms of specificities of the binding and inhibitory capabilities of MYBPH towards ROCK1 and ROCK2. Along line, it is important to note that RhoE binds to ROCK1 but not to ROCK2 and inhibits its function, resulting in loss of stress fiber formation (Riento *et al*, 2003). It was also reported that siRNA-mediated ROCK1 knockdown results in loss of stress fibers, in contrast to lack of such effects in cells knocked down for ROCK2 (Yoneda *et al*, 2005). Together, these findings indicate that ROCK1 plays a major role in stress fiber formation and are in line with the present findings of actomyosin regulation by MYBPH through ROCK1 inhibition.

Considering that ROCK1 also mediates regulatory phosphorylation of various other molecules, such as endothelial nitric oxide synthase (eNOS) and collapsin response mediator protein 2 (CRMP2), and is involved in a wide range of disease states including vasospasms, pulmonary hypertension, and nerve injury (Etienne-Manneville and Hall, 2002; Riento and Ridley, 2003), it would be interesting to investigate whether MYBPH might be involved in such disease states as a regulator of ROCK1. In addition, given that collective cell migration plays an important role in various physiological settings including morphogenesis, tissue regeneration, and repair of wounded epithelial tissues (Kimura *et al*, 1996; White *et al*, 2001; Pogach *et al*, 2007), it is of note that changes in MYBPH expression alter actomyosin organization, and consequently affect collective cell migration, especially when considering that TTF-1 is a master regulatory transcription factor involved in peripheral lung development (Kimura *et al*, 1996; Yatabe *et al*, 2002) and that type II pneumocyte hyperplasia, a reconstitution process of the alveolar lining, is associated with increased TTF-1expression (White *et al*, 2001; Pogach *et al*, 2007).

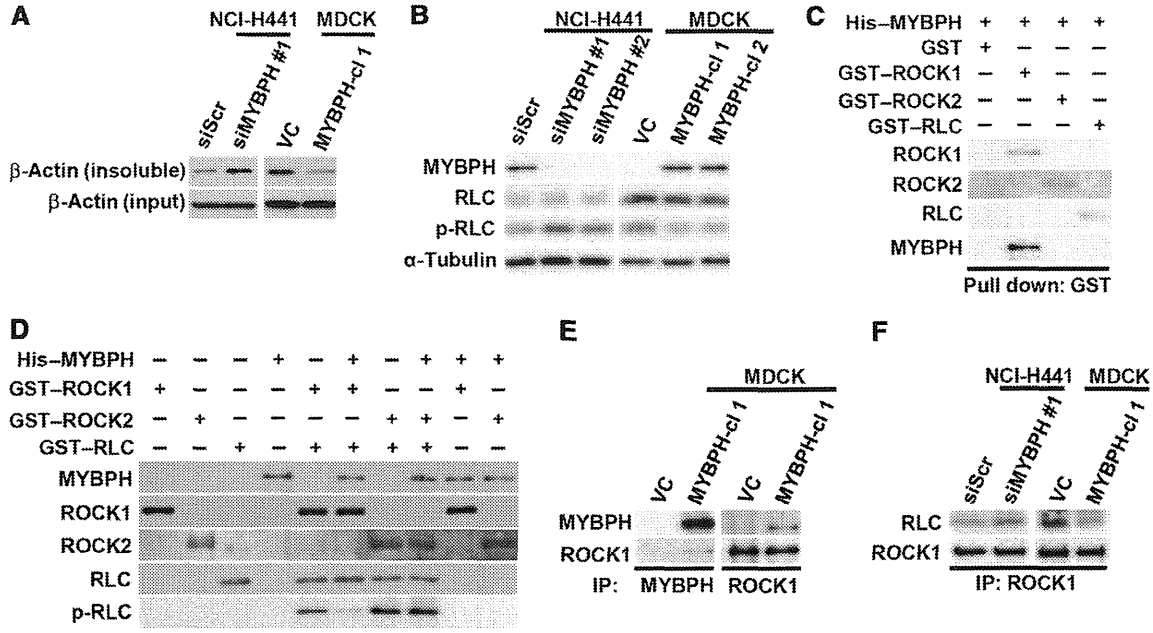

Figure 6 MYBPH inhibits phosphorylation of RLC through interaction with ROCK 1. (**A**) Actin assembly assay showing an increase in triton-insoluble unassembled F-actin (TIF) in siMYBPH-treated NCI-H441 cells as well as opposite effects by MYBPH introduction in MDCK cells. (**B**) Western blot analysis showing induction of RLC phosphorylation by MYBPH knockdown in NCI-H441 cells as well as reduction in MYBPH transfectants of MDCK cells. p-RLC, phospho-RLC (T18/S19). (**C**) *In-vitro* protein–protein binding assay results showing interaction of purified MYBPH with ROCK1, but not with ROCK2 or RLC. (**D**) *In-vitro* ROCK kinase assay using purified RLC protein as a substrate, showing inhibition of ROCK1-mediated RLC phosphorylation by MYBPH. (**E**) Immunoprecipitation–western blot (IP–WB) analysis showing co-immunoprecipitation of MYBPH with ROCK1 in MDCK cells expressing exogenous MYBPH. (**F**) IP–WB analysis showing increased interaction between ROCK1 and RLC by siMYBPH treatment in NCI-H441 cells. Conversely, their reduced interaction was seen in MDCK cells stably transfected with MYBPH. Figure source data can be found with the Supplementary data.

Our results clearly demonstrate that MYBPH negatively regulates cell motility, invasion, and metastasis. Thus, it is quite conceivable that *MYBPH* induction by *TTF-1* is deleterious for lung adenocarcinoma progression, which is thereby inactivated by promoter DNA methylation in a fraction of *TTF-1*-positive lung adenocarcinomas. This finding in turn resolves a question arising from previous observations that a high level of *TTF-1* expression, which we and others have identified as a lineage-survival oncogene in lung adenocarcinoma (Kendall *et al*, 2007; Tanaka *et al*, 2007; Weir *et al*, 2007; Kwei *et al*, 2008), is paradoxically associated with favourable prognosis (Anagnostou *et al*, 2009). We note that during the preparation of this manuscript, Jacks and colleagues reported that TTF-1 downregulation was associated with tumour progression and acquisition of metastatic ability, in association with derepression of HMGA2 in a lung adenocarcinoma model of mutant K-ras/p53 conditional knockout (Winslow *et al*, 2011). Our findings further indicate that MYBPH plays a crucial role as a positively regulated downstream effector of TTF-1, with capabilities for inhibiting cancer cell motility, invasion, and metastasis. Thus, both transcriptional activation and repression by TTF-1 appear to be engaged in conferring a less aggressive phenotype, despite its opposing role as a lineage-survival oncogene in TTF-1-positive lung adenocarcinomas (Kendall *et al*, 2007; Tanaka *et al*, 2007; Weir *et al*, 2007; Kwei *et al*, 2008).

Materials and methods

Cell lines

The derivation, characteristics, and culture conditions of the human lung adenocarcinoma cell lines utilized, and the immortalized human lung epithelial cell line HPL1D as well as the highly metastatic NCI-H460-LNM35 (LNM35) lung cancer cell line were previously reported (Masuda *et al*, 1997; Kozaki *et al*, 2000; Tanaka *et al*, 2007). An MDCK cell line was purchased from RIKEN Cell Bank and maintained in Dulbecco's Modified Eagle's Medium containing 10% fetal bovine serum.

Antibodies, reagents, and oligonucleotide primers

The anti-TTF-1 antibody for western blot analysis was purchased from DAKO; anti-TTF-1 for the ChIP assay from Thermo; anti-MYBPH from Abnova; anti-E-cadherin from BD Transduction Laboratories; anti-GST and anti-His from MBL; anti-NMHC IIA, anti-MLCK, anti-β-actin, and anti-α-tubulin from Sigma-Aldrich; anti-ROCK1, anti-ROCK2, anti-RLC, anti-phospho-RLC (T18/S19), anti-cofilin, anti-phospho-cofilin (S3), anti-phospho-LIMK1 (T508)/LIMK2 (T505), anti-mouse IgG, and anti-rabbit IgG from Cell Signalling Technology; anti-Citron from Novus; anti-RhoA, anti-MRCK-α, and anti-MRCK-β from Santa Cruz; and anti-ZIPK from Calbiochem. ROCK-specific inhibitor Y-27632 was also purchased from Calbiochem. The sequences of the oligonucleotide primers used for PCR and sequencing are provided in Supplementary Table S1.

DNA constructs

The expression construct of full-length human *TTF-1* (pCMV puro-TTF-1) was previously described (Tanaka *et al*, 2007). Full-length human *MYBPH* cDNA (OpenBio) was inserted into a pCMV-puro vector and the entire open reading frame of the resultant construct (pCMVpuro-MYBPH) was thoroughly sequenced. Transfection was performed using FuGENE6 (Roche), followed by puromycin selection.

Microarray data

RNA was extracted from HPL1D cells transiently transfected with TTF-1 or an empty vector followed by puromycin selection for 3 days, and analysed in duplicate (GSE26721), using a low RNA fluorescent linear amplification kit and 44K whole human genome microarrays (Agilent Technologies), essentially as described previously (Tomida *et al*, 2009). Our previously obtained micro-

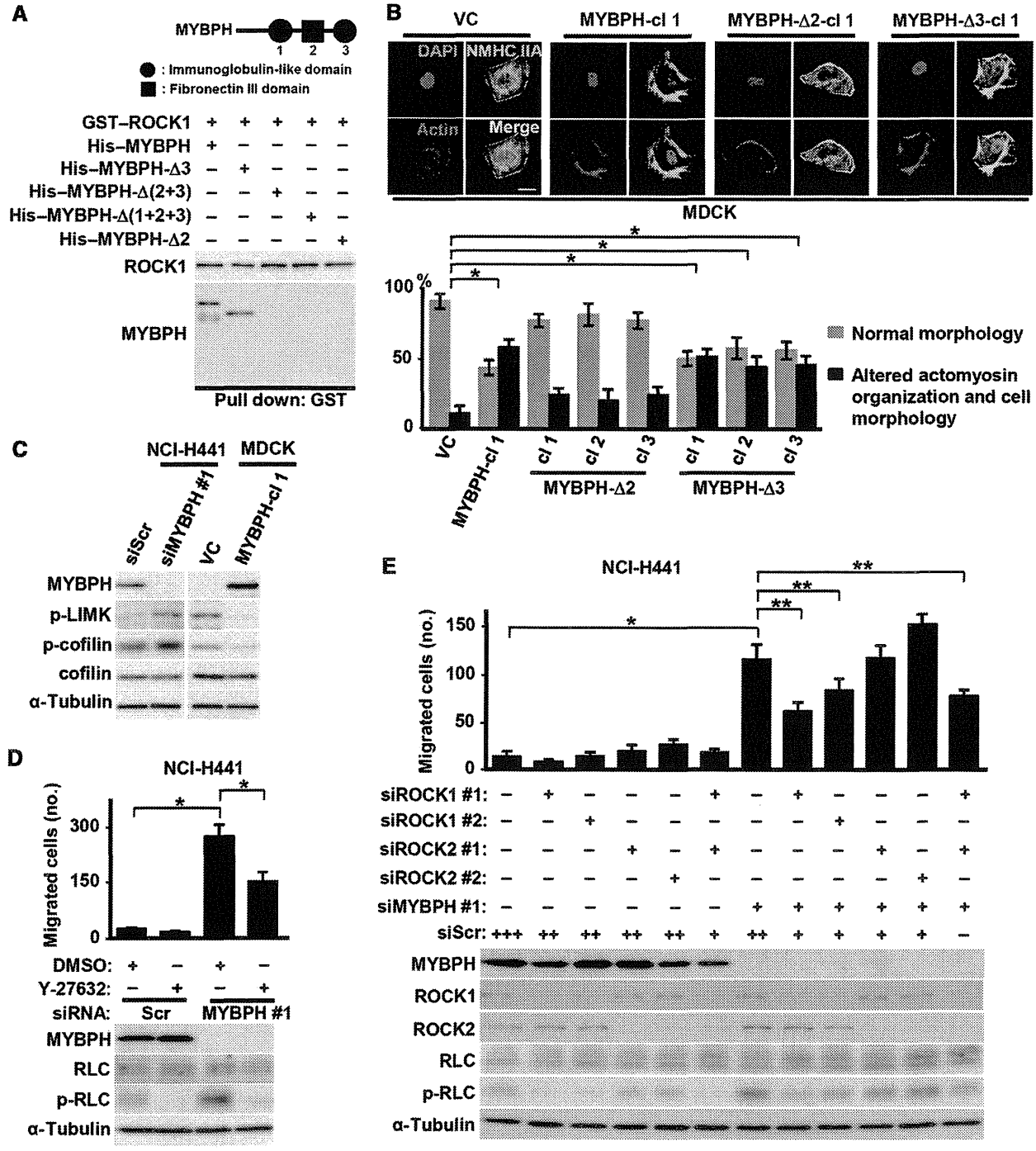

Figure 7 MYBPH knockdown-induced effects on actin bundle formation, cell motility and RLC phosphorylation are alleviated through ROCK1 binding and inhibition. (**A**) Top panel: schematic representation of domain organization of MYBPH. Bottom panel: *in-vitro* protein–protein binding assay showing requirement of a fibronectin type III domain of MYBPH for its binding with ROCK1. Western blot analysis of His-tagged MYBPH-wt, -Δ3, -Δ(2 + 3), -Δ(1 + 2 + 3), and -Δ2 proteins are shown in Supplementary Figure S12. (**B**) Top panels: immunofluorescence staining for DAPI (blue), actin (red), and NMHC IIA (green) in MDCK cells stably introduced with an empty vector (VC), or MYBPH expression constructs of wild-type or deletion mutants lacking either fibronectin type III (MYBPH-Δ2) or immunoglobulin-like domains. Bars indicate 10 μm. Bottom panel: proportions of cells according to morphology, which were determined as shown in Figure 5A. Bars, mean ± s.d.; $^{*}P<0.001$. (**C**) Western blot analysis showing induction of LIMK and cofilin phosphorylation by MYBPH knockdown in NCI-H441 cells as well as reduction in MYBPH transfectant of MDCK cells. p-LIMK, phospho-LIMK1 (T508)/LIMK2 (T505); p-cofilin, phospho-cofilin (S3). (**D**) Top panel: partial cancellation of the MYBPH knockdown-induced motility by a simultaneous treatment with a ROCK-specific inhibitor Y-27632 in NCI-H441 cells. Bars, mean ± s.d.; $^{*}P<0.01$. Bottom panel: representative western blot images for RLC phosphorylation. (**E**) Top panel: partial cancellation of MYBPH knockdown-induced motility by simultaneous treatment with siRNAs against ROCK1 in NCI-H441 cells. Bars, mean ± s.d.; $^{*}P<0.01$; $^{**}P<0.05$. Bottom panel: representative western blot images for RLC phosphorylation. siRNA concentrations: +, 40 nM; + +, 80 nM; + + +, 120 nM. Figure source data can be found with the Supplementary data.

array data of 90 lung adenocarcinoma cases (Takeuchi *et al*, 2006; GSE11969) were used to analyse the association of *MYBPH* expression with *TTF-1* expression as well as with various clinical parameters.

siRNA treatment

siRNA duplexes targeting TTF-1 (siTTF-1) and MYBPH (siMYBPH #1 and #2 as well as siMYBPH-AF488, Alexa Fluor 488-conjugated siMYBPH #1) and a negative control (siScr) were obtained from

Sigma Genosys, while siRNA duplexes targeting ROCK1 (siROCK1 #1 and #2) and ROCK2 (#1 and #2) from Invitrogen. Transfection of each siRNA at 40 nM was performed using Lipofectamine RNAi-MAX (Invitrogen). Cells were harvested at 48 h after transfection for each assay. The sequences of the siRNAs are provided in Supplementary Table S1.

Western blot analysis

Western blot analysis was performed according to standard procedures using Immobilon-P filters (Millipore) and an Enhanced Chemiluminescence system (GE Healthcare). NCI-H441 cells were treated with Y-27632 (5 μM) for 15 min before.

IP–WB analysis

Cells (2×10^7) were lysed with modified RIPA buffer containing protease inhibitor cocktail Tablets (Roche) and incubated with each antibody overnight at 4°C, followed by addition of protein G Sepharose (GE Healthcare) and subsequent incubation for an additional 1 h. The immunoprecipitates were analysed by western blot analysis.

Dual-luciferase reporter assay

An MYBPH *luciferase* reporter construct was generated using a pGL4 basic reporter vector (Promega) and a PCR-amplified 1.0-kb genomic fragment from the MYBPH promoter region. Mutant vectors carrying deletions at the predicted binding sites for *TTF-1* and *NKX2-5* were constructed using a QuikChange site-directed mutagenesis kit (Stratagene). HPL1D cells (3.0×10^5) transiently expressing *TTF-1* were transfected with each pGL4 vector (1.8 μg) together with a pRLTK vector (0.2 μg), then the cell lysates were collected after 48 h. Luciferase reporter activities were determined using a Dual-Luciferase Reporter Assay System (Promega). Firefly luciferase activity was normalized with that of Renilla luciferase.

ChIP assay

NCI-H441 cells (1.0×10^8) were harvested after crosslinking with 1% formaldehyde. Chromatin was sheared by sonication to an average length of 500–600 bp, followed by immunoprecipitation with a TTF-1-specific antibody. After reversal of crosslinking, immunoprecipitated chromatin was subjected to PCR using primers for the predicted binding sites of *TTF-1* and *NKX2-5* as well as those for an unrelated genomic region as a negative control.

Treatment with 5-aza-2′-deoxycytidine

Cells ($1.0–1.5 \times 10^5$) were incubated with 1 or 2 μM of 5-aza-2′-deoxycytidine (5-Aza-dC; Sigma) for 5 days. Media were changed every 24 h. Semiquantitative PCR was performed using primers for amplification of the coding region of MYBPH.

Bisulphite sequencing analysis

Bisulphite conversion of genomic DNA was performed using MethylEasy Xceed™ (Human Genetic Signatures), according to the manufacturer's instructions. The MYBPH promoter region was amplified using nested primers and the resultant PCR products were cloned into pGEM-T easy vectors (Promega), followed by sequencing of randomly selected clones.

Laser microdissection and MSP

Cancer cells were microdissected from 20 μm thick frozen sections using a Leica LMD 7000 Laser Micro-dissection system (Leica Microsystems). Bisulphite-modified DNA was used as a template for SYBR Green (Applied Biosystems)-based real-time PCR, with primers designed for specific detection of methylated DNA at a CpG (#8) close to the TTF-1-binding consensus sequence of the *MYBPH* promoter and a promoter region without CpG sites of the reference gene, *ACTB*. The methylation level in the *MYBPH* promoter was determined as the ratio of methylation-specific PCR-amplified *MYBPH* gene to *ACTB* reference gene, and then multiplied by 1000 for easier tabulation.

In-vitro motility, invasion, scratch, and MTT assays

In-vitro motility and invasion assays were essentially performed as previously described (Kozaki *et al*, 2000). For each assay, 1×10^5 MDCK cells, 1.5×10^5 NCI-H441, and HPL1D cells were added to the upper chambers, then incubated for 24, 36 and 36 h, respectively. NCI-H441 cells were treated with Y-27632 (5 μM) for 15 min before incubation. For a scratch assay, 1.5×10^6 cells were plated in 6-well plates. After 24 h of incubation, a single linear wound was created with a 200-μl pipette tip. An MTT assay was performed with TetraColor One (Seikagaku) according to the manufacturer's instructions.

Three-dimensional Matrigel invasion assay and immunostaining

One hundred microlitres of Matrigel (BD Biosciences) was prepared on 18×18 mm coverslips in 6-well plates, on which 2×10^5 cells were plated and cultured for 48 h, followed by fixation with 3.7% formaldehyde for 30 min and post-fixing with 0.1% Triton X-100 for 30 min at room temperature (RT). Cells were incubated with blocking buffer (1% BSA in PBS) overnight at 4°C and were visualized by staining with Alexa-conjugated phalloidin (Molecular Probes). The coverslips were mounted onto slides using Fluoromount (Diagnostic BioSystems) and analysed using an A1 Rsi confocal microscope (Nikon). The invasion distance was defined as that between the slide glass (top of the Matrigel) and the centre of fluorescence intensity, and measured using MetaMorph (Molecular Devices) software. The extent of collective cell migration was defined as the ratio of collective cells ($\geqslant 5$ cells) to total cell number. Data shown represent three independent experiments, with >100 cells counted in each.

In-vivo metastasis assay

LNM35 cells (1.0×10^7) in 0.1 ml of serum-free RPMI-1640 medium were injected into subcutaneous tissues of the right groin of 6-week-old female SCID mice. Forty days after inoculation, the mice were euthanized, and their lungs and subcutaneous tumours resected, weighed, and fixed with 10% formaldehyde. Lung-metastatic nodules were examined under a dissecting microscope. An experimental metastasis assay following tail vein injection of tumour cells was performed, essentially as described by Shibue and Weinberg (2009). NCI-H441 cells were transfected with either Alexa Fluor 488-conjugated siScr (siScr-AF488) or -siMYBPH #1 (siMYBPH-AF488) as described above, then the transfectants were harvested 48 h later. Cells at 1.0×10^6 in 0.1 ml of PBS were injected into tail veins of 6-week-old female SCID mice. Five days after injection, the mice were euthanized, then 6 ml of PBS was injected into the right ventricle for perfusion of the lung microvasculature. The perfused lungs were embedded in OCT (Sakura), sectioned (thickness 10 μm) with a Leica CM3050 (Leica Microsystems), and fixed using Fluoromount. Perfusion-resistant cells were determined by direct counting in the sections using an A1 Rsi confocal microscope.

Immunostaining

Cells (0.5×10^5) were plated on 18×18 mm coverslips in 6-well plates and cultured for 12 h. NCI-H441 cells were treated with Y-27632 (5 μM) for 15 min before plated. The cells were fixed by incubating with 3.7% formaldehyde for 10 min at RT, followed by post-fixing with 0.1% Triton X-100 for 10 min at RT. Cells were incubated with blocking buffer overnight at 4°C, followed by another incubation with antibodies (diluted in blocking buffer) for 60 min at RT. After treatment with Alexa-conjugated secondary antibodies (Molecular Probes) for 60 min at RT, the coverslips were mounted onto slides using Fluoromount, and analysed using an A1 Rsi confocal microscope.

Actin assembly assay

Cells were lysed with buffer containing 1% Triton X-100, 10 mM EGTA, 40 mM NaCl, 10 mM imidazole, and a protease inhibitor cocktail (Roche) at 4°C. The lysates were centrifuged at $15\,000 \times g$ for 5 min at 4°C, then the pellets were washed, dissolved in 1 × SDS sample buffer, and subjected to western blot analysis with an anti-actin antibody. Three independent experiments were performed in triplicate, with similar results obtained.

Preparation of recombinant proteins

His-tagged MYBPH-wt, -Δ3, -Δ(2 + 3), -Δ(1 + 2 + 3), and -Δ2 proteins were expressed in Sf9 insect cells using a Gateway system (Invitrogen), according to the manufacturer's instructions. Recombinant His-tagged MYBPH-wt, -Δ3, -Δ(2 + 3), -Δ(1 + 2 + 3), and -Δ2 proteins were purified using imidazole-affinity chromatography. Recombinant GST-tagged ROCK1 (amino acids 17–535) and GST-tagged ROCK2 (amino acids 5–554) were purchased from Sigma. GST-tagged RLC and GST were from Abnova.

In-vitro protein–protein binding assay

Purified His-tagged MYBPH-wt, -Δ3, -Δ(2 + 3), -Δ(1 + 2 + 3), or -Δ2 was mixed with glutathione beads coated with recombinant GST, GST-tagged RLC, GST-tagged ROCK1, or GST-tagged ROCK2. After repeated washes with a solution containing 20 mM MOPS (pH 7.2), 1 mM dithiothreitol, 5 mM EGTA, 25 mM β-glycerophosphate, 1 mM Na_3VO_4, and 75 mM $MgCl_2$, the bound proteins were eluted and subjected to SDS–PAGE, followed by western blot analysis with anti-ROCK1, anti-ROCK2, anti-RLC, or anti-MYBPH antibodies.

In-vitro kinase assay

Purified GST-tagged RLC, GST-tagged ROCK1, and GST-tagged ROCK2 were incubated in phosphorylation buffer (25 mM Tris–HCl (pH 7.5), 5 mM $MgCl_2$, and 0.5 mM ATP) with or without purified His-tagged MYBPH at a final protein concentration of 0.1 μM for 1 h at 37°C. The reactions were analysed by SDS–PAGE, followed by western blot analysis with anti-phospho-RLC antibodies. For detection of phosphorylations, we used an *in-vitro* kinase assay, in which those proteins were incubated in kinase buffer containing 100 μm [γ-^{32}P]ATP (2 μCi), then resolved by SDS–

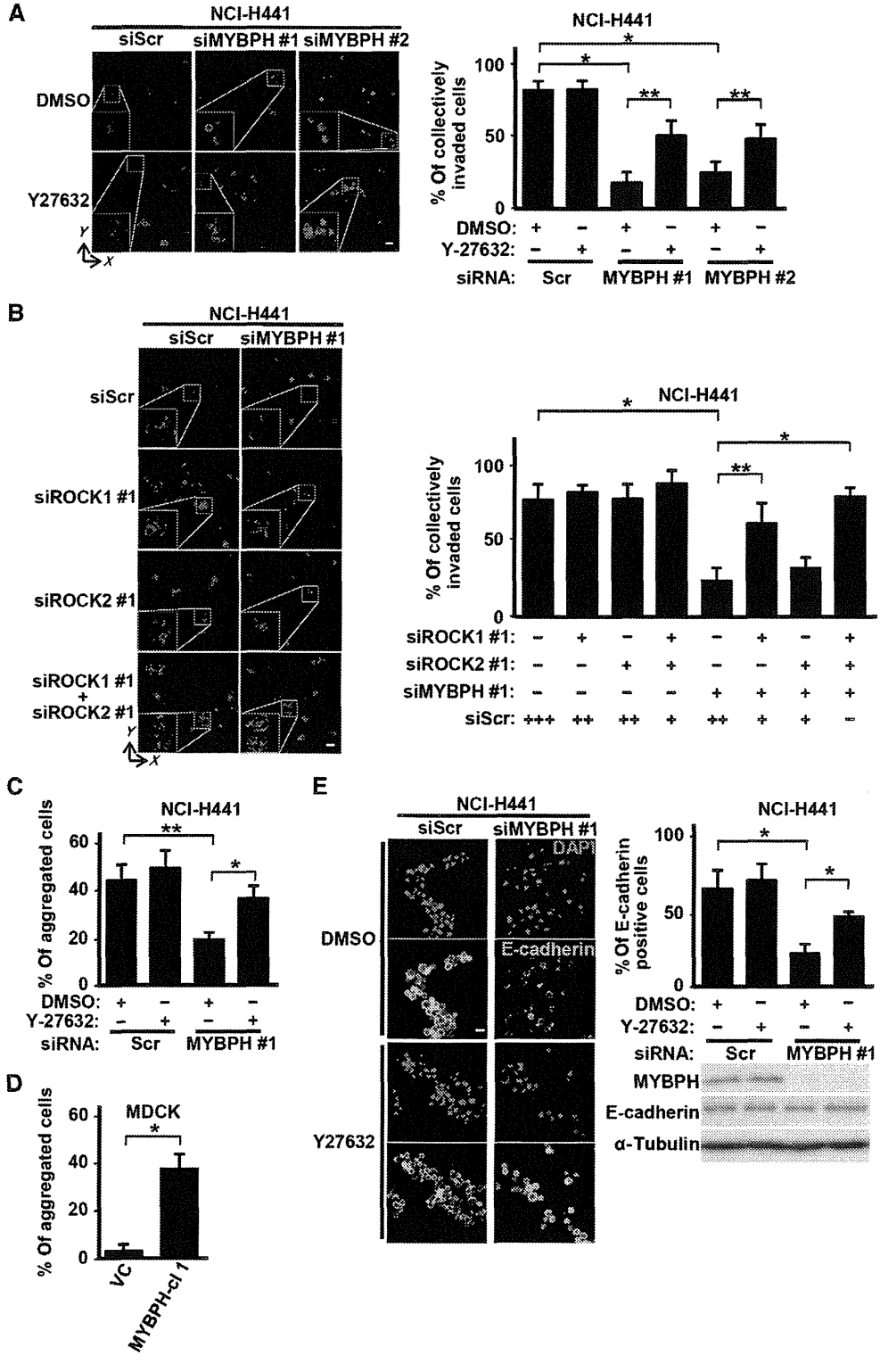

PAGE and stained with CBB reagents. Radiolabelled phosphoprotein bands were visualized by autoradiography of a dried gel.

Cell aggregation assay

Cells (1×10^6) were suspended in RPMI or DMEM medium supplemented with 10% FBS in 12-well plates pre-coated with 2% BSA (Roche), then cultured with horizontal rotation (75–100 r.p.m.) at 37°C for 30 min. Aggregation was fixed by adding 2% glutaraldehyde (Nacalai Tesque). The extent of aggregation ($\geqslant 5$ cells) was defined as the ratio of total particle number to initial cell number. Cells were then attached onto a slide glass using a *CYTOSPIN* device (2000 r.p.m., 5 min) followed by immunostaining, or were dissolved in 1 × SDS sample buffer, then subjected to western blot analysis. Cells with intense staining on the cell surface, as shown by MetaMorph software finding, were considered to be E-cadherin positive. Data shown represent three independent experiments, with >100 cells counted in each.

Statistical analysis

Statistical analyses of data presented in Figures 2B and 4F were performed using Fisher's exact test. For the other experiments, significance levels were determined by a *t*-test. All statistical analyses are performed in a two-sided manner.

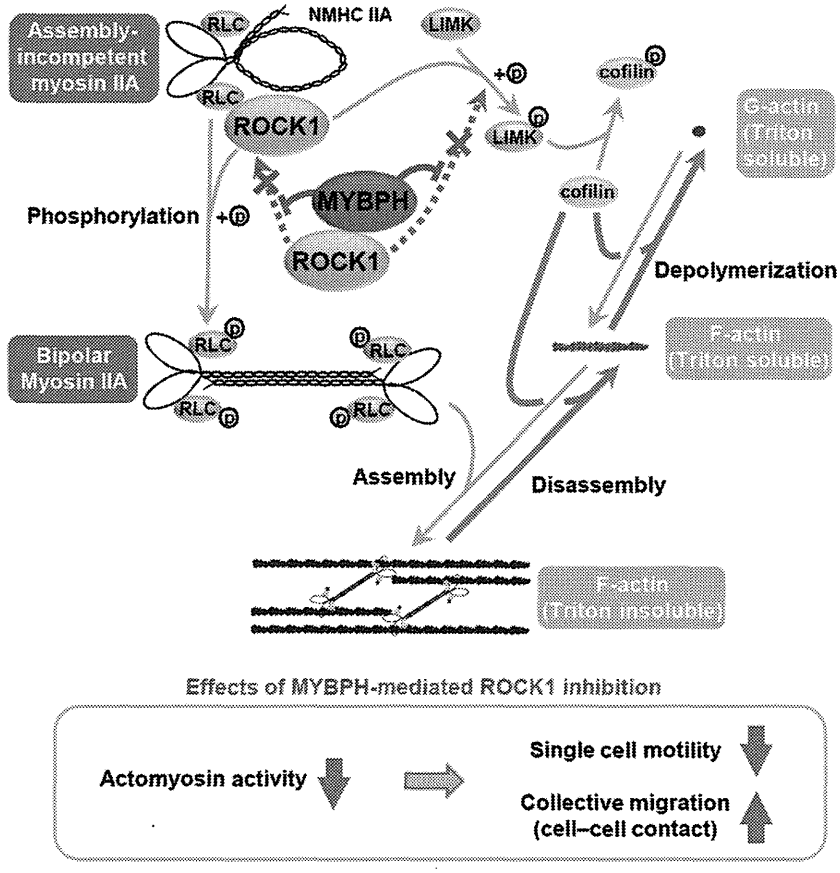

Figure 9 Schematic diagram demonstrating how MYBPH affects actomyosin organization through inhibition of ROCK1. RLC phosphorylation-mediated bipolar NM IIA formation, a prerequisite for actomyosin assembly, is disturbed by MYBPH via direct interaction with and negative regulation of ROCK1, which also leads to inhibition of the LIMK–cofilin pathway. Consequently, MYBPH inhibits ROCK1-driven actomyosin organization, which in turn reduces single cell motility and promotes collective cell migration.

Figure 8 MYBPH knockdown reduces cell–cell contact and collective cell migration. (**A**) Three-dimensional Matrigel invasion assay findings showing decreased collective cell migration by MYBPH knockdown and significant reversion by simultaneous Y-27632 treatment in NCI-H441 cells. Cells were visualized by actin staining (red). White bars indicate 50 μm. The proportions of cells with collective invasion were evaluated as in Figure 3D. Data shown represent three independent experiments. Bars, mean ± s.d.; $*P<0.01$. (**B**) Three-dimensional Matrigel invasion assay findings showing decreased collective cell migration by MYBPH knockdown and significant reversion by simultaneous siROCK1 treatment in NCI-H441 cells. Cells were visualized by actin staining (red). White bars indicate 50 μm. The proportions of cells with collective invasion were evaluated as in Figure 3D. Data shown represent three independent experiments. Bars, mean ± s.d.; $*P<0.01$.; $**P<0.05$. siRNA concentrations: +, 40 nM; + +, 80 nM; + + +, 120 nM. (**C**) Cell aggregation assay findings showing that MYBPH knockdown decreased formation of cell aggregates and significant reversion by simultaneous Y-27632 treatment in NCI-H441 cells. The proportions of aggregated cells were evaluated as described in Materials and methods. Data shown represent three independent experiments. Bars, mean ± s.d.; $*P<0.05$; $**P<0.01$. (**D**) Cell aggregation assay findings showing increased numbers of cell aggregates in stable MYBPH transfectants of MDCK cells. Data shown represent three independent experiments. Bars, mean ± s.d.; $*P<0.01$. (**E**) Immunofluorescent staining of E-cadherin in NCI-H441 cells subjected to cell aggregation assay. Cells were stained with anti-E-cadherin antibody (green) and DAPI (blue), which revealed decreased cell surface E-cadherin expression in NCI-H441 cells knocked down for MYBPH. Note that cell aggregation was also decreased by siMYBPH treatment and these phenotypic changes were significantly reverted when the cells were simultaneously treated with Y-27632. Western blot analysis findings showed negligible changes in total amounts of E-cadherin. Bar indicates 10 μm. Proportions of E-cadherin-positive cells were evaluated as described in Materials and methods. Data shown represent three independent experiments. Bars, mean ± s.d.; $*P<0.01$. Figure source data can be found with the Supplementary data.